Acta Cryst. (1995). B51, 880–888

Structure at 140 K, Lattice Dynamics and Phase Transition of 4,4′-Dichlorobenzophenone

BY F. J. ZÚÑIGA

Departamento de Física de la Materia Condensada, Facultad de Ciencias, Universidad del Pais Vasco, Aptdo 644, 48080 *Bilbao, Spain*

AND A. CRIADO

Instituto de Ciencia de Materiales and Departamento de Física de la Materia Condensada, Consejo Superior de Investigaciones Científicas, Universidad de Sevilla, Aptdo 1065, 41080 *Sevilla, Spain*

(*Received* 8 *July* 1994; *accepted* 8 *February* 1995)

Abstract

The crystal structure of the low-temperature phase of 4,4′-dichlorobenzophenone, $C_{13}H_8Cl_2O$, has been determined at 140 K. Crystal data: $T = 140$ K, $M_r = 251.1$, monoclinic, $I2/c$, $a = 24.62(1)$, $b = 6.091(1)$, $c = 7.476(2)$ Å, $\beta = 100.14(3)°$, $V = 1104(2)$ Å^3, $Z = 4$, $D_x = 1.510$ Mg m^{-3}, λ(Mo $K\alpha$) = 0.7107 Å, $\mu = 0.55$ mm^{-1}, $F(000) = 512$, $R = 0.041$, $wR = 0.050$. A mechanism for the sequence of phase transitions is proposed and a semi-empirical atom–atom potential model has been adopted in order to study the energetic stability of the high- and low-temperature crystal phases. A lattice-dynamical model allowing for molecular internal degrees of freedom has been developed in order to interpret the experimental Raman spectra of both phases.

1. Introduction

Many organic molecular crystals exhibit phase transitions related to the conformational changes of their molecules. Particularly, crystals of molecules with phenyl groups where conformational changes involve incommensurate modulations of the phenyl-group torsional angles are attractive systems. Examples of these systems are biphenyl ($C_{12}H_{10}$), which is one of the most extensively studied compounds (Cailleau, 1986), and, more recently, 4,4′-dichlorobiphenyl sulfone, $(C_6H_4Cl)_2SO_2$ (Pusiol, Wolfenson & Brunetti, 1989; Zúñiga, Pérez-Mato & Breczewski, 1993). Both compounds have a soft-mode mechanism connected to their transitions and despite the difference in the sequence of transitions, it is expected that the competition between intramolecular and intermolecular forces is at the origin of the structural instabilities. In this sense, the proposed empirical models for the intra- and intermolecular interactions could explain the main features of the lattice dynamics in both compounds (Plakida, Bielushkin, Natkaniec & Wasiutynski, 1983; Ishii, Nakayama, Sakato & Kano, 1992).

The compound 4,4′-dichlorobenzophenone, $(C_6H_4Cl)_2CO$ (hereafter DCBP), is monoclinic at room temperature, $C2/c$, $a = 25.161$, $b = 6.104$, $c = 7.535$ Å, $\beta = 101.98°$ and $Z = 4$, and has a structure based on molecules with two non-coplanar phenyl rings (Shields & Kennard, 1977; Granger & Coillot, 1985). It exhibits two phase transitions in the temperature range 160–190 K. The sequence of transitions and the different phases have been studied by means of Raman spectroscopy (Peretti & Ranson, 1979), calorimetry and Brillouin scattering (Ecolivet, Bertault, Mierzejewski & Collet, 1987). The evolution of the Raman spectra from 293 to 6 K confirms that the low-temperature phase is reached through an intermediate phase where new Raman lines appear and then progressively vanish. From the Raman spectra these changes, which seem to keep the C_2 molecular symmetry, are suspected to be due to conformational changes on the relative positions of the phenyl rings. For both transitions, thermal hysteresis phenomena have been reported, pointing to a first-order character of the transitions (Peretti & Ranson, 1979).

However, the Raman studies on DCBP do not show the presence of any soft mode, although a complete knowledge of the dispersion curves would be necessary in order to look for any soft mode off the Brillouin zone centre and to establish whether a different mechanism for the phase transition may be expected from those found in the previous compounds. A Raman study as a function of pressure has also been carried out (Kirin & Pawley, 1982). These authors find anomalies in the Raman frequency dependence with pressure at *ca* 5 kbar (5×10^8 Pa), which they associate with the possible existence of a pressure-induced phase transition which they also attribute to conformational changes related to the phenyl rings. In fact, this pressure-induced transition could be very likely similar to that induced by cooling, resulting in a $p - T$ phase diagram, as seems to be the case in the ferroelastic phase transition of phenothiazine (Criado & Luty, 1993), a molecular compound which also displays molecular conformation changes during the transition.

ISSN 0108-7681

More recently, Wolfenson, Pusiol & Brunetti (1990), using ^{35}Cl NQR spectroscopy, have confirmed that phase transitions occur at 186 and 175 K, respectively (on cooling), and, based on the temperature behaviour of the NQR line-shape, they propose that the intermediate phase ($175 < T < 186$ K) could have an incommensurate structure. The phase transition temperatures were shown to be dependent on the thermal history. The authors also associate the mechanism giving rise to the intermediate phase with changes in the molecular conformation related to twisting of the phenyl groups.

In this paper, the crystal structure of the low-temperature phase of DCBP at 140 K has been determined with X-ray diffraction. Also, a packing energy analysis of the known crystal structures of DCBP has been undertaken using semi-empirical atom–atom functions in order to study the relative energy stability of these phases. This potential energy model has been applied to develop a lattice-dynamical model which allows one to obtain the dispersion curves of both the low- and high-temperature phase in order to discuss the structural stability of both phases. This model also allows one to interpret the experimental Raman spectra satisfactorily. These results allow us to discuss a mechanism which explains the sequence of phase transitions in DCBP.

2. Structural analysis

2.1. *Experimental*

Colourless crystals of DCBP were obtained by slow evaporation from a benzene solution of the purified compound (commercially available). A set of precession photographs was taken at different temperatures within the stability range of the intermediate phase and at 140 K. Temperature was controlled using an open-flow gas cryostat (Cosier & Glazer, 1986).

In the following, the cell at room temperature will be referred to as the basic cell and used for the description of the diffraction patterns. The photographs of the intermediate phase show monoclinic symmetry with the same basic cell. The lattice is no longer C-centred but primitive, and a new type of reflection located close to $1/2\mathbf{a}^*$ off the primitive lattice points appears on layers (hkl) l = odd. The same primitive lattice points appear in the diffraction patterns at 140 K, which also show monoclinic symmetry, but the superlattice reflections disappear and the lattice becomes I-centred, with systematic absences compatible with the $I2/c$ space group (indexing reflections with the same lattice basis given to describe the structure at room temperature).

A more careful study of the shape and temperature behaviour of some reflections in the intermediate phase was carried out on an automatic four-circle diffractometer. The results confirm that the superlattice reflections are not exactly located at $1/2\mathbf{a}^*$ and they can be better indexed according to diffraction vectors $\mathbf{H} = h\mathbf{a}^* + k\mathbf{b}^* + l\mathbf{c}^* + m\mathbf{q}$, with $\mathbf{q} = 0.53\mathbf{a}^*$ and so considered as satellite reflections of the basic primitive lattice. These reflections exhibit large profiles; the $\mathbf{q}$ vector does not vary appreciably with temperature, but their intensities vary strongly. Although these features could not be exactly reproduced on different cooling and heating runs, they indicate an incommensurate nature for the intermediate phase.

Table 1. *Summary of crystal data and data collection parameters*

Crystal form	Prismatic
Crystal size (mm)	0.3 × 0.37 × 0.4
Temperature (K)	140
Reflections for lattice parameters	25 ($10 \le \theta \le 16°$)
Cell parameters	
a (Å)	24.62 (1)
b (Å)	6.091 (1)
c (Å)	7.476 (2)
β (°)	100.14 (3)
Space group	$I2/c$
$(\sin\theta/\lambda)_{max}$ (Å^{-1})	0.904
h, k, l limits	(±44, 11, 13)
Scan width (°)	$0.75 + 0.34\tan\theta$
Scan speed (° min^{-1})	0.92–2.75
No. of measured reflections	3968
No. of independent reflections ($I \ge 3\sigma$)	3413 (2217)
No. of contributing reflections	2871
No. of variables	91
R_{int} without absorption correction	0.043
Weights	$1/\sigma^2(F)$
R	0.041
wR	0.050
GOF	1.83
Max. shift/e.s.d.	0.03

Another important feature of this phase is the temperature behaviour of the intensities of main reflections of the basic lattice. It has been found that reflections (hkl) with $h + k = 2n + 1$ and $h + k + l = 2n$ increase intensity during cooling, whereas those reflections with $h + k = 2n$ and $h + k + l = 2n + 1$ decrease in intensity. The first group of reflections are compatible with an I-centred symmetry but violate the systematic absences of a C-centred lattice, whereas the second group have the contrary characteristics. Such behaviour allows us to conclude that during the intermediate phase there is a continuous evolution from the room- to the low-temperature structure.

2.2. *Structure at* 140 K

Crystal data and data collection parameters of the lower temperature phase are summarized in Table 1. Intensities were collected with a CAD-4 diffractometer equipped with the cryostat described above. Temperature stability was maintained within ±0.2 K during the time of measurement. Measurement stability was checked by recording three check reflections every 2 h. At the end of the measurements the reflections did not show significant changes. Data reduction, averaging of symmetry equivalent reflections and refinements were carried out using the program system *XRAY*72 (Stewart, Kruger, Ammon, Dickinson & Hall, 1972).

Table 2. *Atomic coordinates and equivalent thermal displacements (isotropic for* H *atoms; e.s.d.'s are given in parentheses)*

	x	y	z	U_{eq}
Cl	0.21480 (1)	0.50766 (5)	0.79771 (4)	0.03075 (9)
O	0	−0.1842 (2)	0.75	0.0311 (4)
C(1)	0.05326 (4)	0.1412 (2)	0.7612 (1)	0.0154 (2)
C(2)	0.05500 (5)	0.3497 (2)	0.6827 (1)	0.0178 (2)
C(3)	0.10493 (5)	0.4600 (2)	0.6902 (1)	0.0192 (3)
C(4)	0.15303 (5)	0.3613 (2)	0.7790 (1)	0.0195 (3)
C(5)	0.15291 (4)	0.1521 (2)	0.8561 (2)	0.0202 (3)
C(6)	0.10269 (4)	0.0425 (2)	0.8457 (1)	0.0179 (2)
C(7)	0	0.0173 (2)	0.75	0.0178 (3)
H(2)	0.0205 (6)	0.419 (3)	0.620 (2)	0.027 (4)
H(3)	0.1038 (6)	0.605 (2)	0.635 (2)	0.024 (4)
H(5)	0.1846 (7)	0.090 (3)	0.912 (2)	0.045 (5)
H(6)	0.1002 (6)	−0.098 (2)	0.899 (2)	0.023 (4)

Table 3. *Interatomic bond distances* (Å) *and angles* (°)

Cl—C(4)	1.747 (1)	C(2)—C(1)—C(6)	119.22 (9)
C(1)—C(2)	1.403 (1)	C(2)—C(3)—C(4)	118.9 (1)
C(2)—C(3)	1.393 (2)	C(3)—C(4)—C(5)	121.9 (1)
C(3)—C(4)	1.388 (2)	C(4)—C(5)—C(6)	118.66 (9)
C(4)—C(5)	1.399 (2)	C(5)—C(6)—C(1)	120.6 (1)
C(5)—C(6)	1.395 (2)	C(1)—C(7)—O	120.15 (6)
C(6)—C(1)	1.404 (1)	C(1)—C(7)—C(1^{i})	199.7 (1)
C(1)—C(7)	1.502 (1)		
C(7)—O	1.227 (2)		

Symmetry code: (i) $-x, y, \frac{3}{2} - z$.

The structure was refined using the starting parameters from the room-temperature structure. The refinement was based on $|F|$ and performed in the full-matrix mode. Scattering factors for neutral atoms and anomalous dispersion corrections were taken from *International Tables for Crystallography* (1974, Vol. IV). The non-H atoms were refined with anisotropic thermal displacements. A difference-Fourier synthesis revealed all H atoms, which were subsequently included in the refinement with isotropic thermal parameters. The final atomic parameters including equivalent isotropic thermal displacements are given in Table 2* and the bond distances and angles are listed in Table 3.

A drawing of the DCBP molecule and projections along the *b*-direction of the structure at room temperature and at 140 K are shown in Figs. 1 and 2. The DCBP molecules lie on twofold special positions with the C(7)—O bond along the binary axis. The phenyl rings are almost planar [maximum distance 0.011 Å from C(4) to the least-squares plane]. The conformational configuration of the DCBP molecule, defined by the bending angle (φ) C(1)—C(7)—C(1′) [C(1′) related to C(1) by the molecular twofold axis] and the dihedral angle (θ) between the plane of the aromatic ring and the plane defined by the C(1), C(7) and C(1′) atoms, is similar in both phases. Values of these angles are 119.7 and 27.8° (121.0 and 25.1° at room temperature), respectively. Bond distances and angles are comparable in both phases also. The structure of this compound can be described as linear chains of molecules stacked along the *b*-direction. These stacks are arranged in rows parallel to the *c*-direction at $x = 0$ and $x = 1/2$ with the molecules also parallel to each other so that the molecular C(7)—O bonds for consecutive stacks in the row point to opposite sides along the *b*-direction. The structure of these rows is practically identical for both phases, except that their packing obeys to a *C*- (room-temperature phase) or *I*-centred (140 K) Bravais lattice. The four shorter intermolecular Cl···Cl distances range from 3.559 to 3.739 Å in the 140 K structure, whereas the corresponding values in the room-temperature structure are 3.714 and 3.773 Å.

3. Crystal energy and lattice-dynamical model

The use of semi-empirical 6-exp atom–atom potential functions to model the intermolecular crystal energy in molecular crystals has proved to be fruitful (Pertsin & Kitaigorodsky, 1987). In our case, we have adopted potential parameters taken from the literature among those which have turned out to be more successful in the past. For C—C, C—H and H—H interactions we have selected Williams' (1967) parameters, for O interactions those of Cox, Williams & Hsu (1981), whereas for Cl

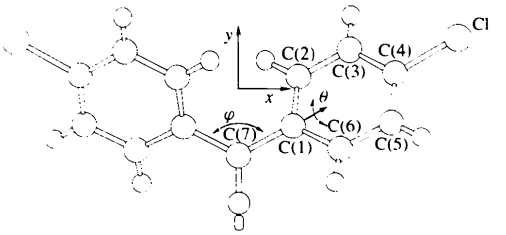

Fig. 1. Drawing of the DCBP molecule. *x*–*y* axes (*z* would complete a right-handed orthogonal frame) indicate the orientation of the principal inertia frame at the centre of mass of the molecule. (θ) and (φ) refer to the bending and the phenyl twist angles, respectively.

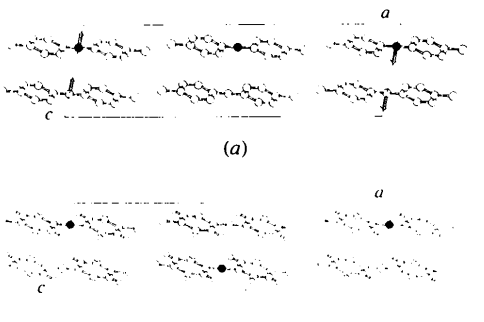

Fig. 2. (*ac*)-Projection of the structure at (*a*) room temperature and (*b*) 140 K. Full and empty circles represent C(7)—O groups pointing up and down, respectively. Arrows indicate the $\frac{1}{2}c$ molecular displacements which transform the room-temperature into the low-temperature structure.

* Lists of structure factors, anisotropic displacement parameters and H-atom coordinates have been deposited with the IUCr (Reference: HR0007). Copies may be obtained through The Managing Editor, International Union of Crystallography, 5 Abbey Square, Chester CH1 2HU, England.

interactions the potential parameters of Bates & Busing (1974) were chosen. The mixed interactions between different potential sets were calculated using combination rules for $V(r) = -A/r^6 + B\exp(-Cr)$ so that the mixed A parameter can be obtained as the geometric mean of the pure ones, the arithmetic mean applies to the C parameter and B for the mixed interactions have been obtained so that the potential curve minimum is located at the arithmetical mean of the potential minima of the corresponding pure interactions. Our choice of potential parameters is based on those sets which have been sufficiently tested for lattice dynamical purposes in the literature and also by our own experience (Muñoz & Criado, 1992; Criado & Muñoz, 1993), indicating that the newer potential sets are not always better, as is the case for Williams & Starr's (1977) potential set for C and H interactions which gave poorer lattice dynamical results (Criado & Marquez, 1988) than Williams' (1967) set. A recent set for heteroatoms has been developed using a very large compound database (Filippini & Gavezzotti, 1993) and its performance for lattice-dynamical calculations should be studied, although the authors report that they find results for hydrocarbons similar to those obtained with Williams' (1967) parameters.

The rigid-body approximation does not hold strictly for DCBP because low-frequency internal modes are expected to appear overlapping with the rigid-body lattice modes. Therefore, it is necessary to consider molecular internal degrees of freedom and consequently, a model for the intramolecular contribution to the crystal is called for. In order to simplify the problem, we will consider only those internal coordinates which are expected to couple to the lattice modes because they are involved in the low-frequency molecular modes. In our case, we have considered three internal degrees of freedom, both phenyl rotations around the C(7)—C(1) bond and the change of the bending angle (φ) C(1)—C(7)—C(1′) between both phenyl groups (see Fig. 1); the phenyl groups themselves have been considered as rigid in this model because their frequency is expected to be much higher than that of the lattic modes. For the intramolecular energy we have chosen the simplest model in which this contribution is obtained as the sum of all intramolecular atom–atom terms with the same function used for the intermolecular region. In this way, the atom–atom interaction between the phenyl rings will determine their relative orientation in the isolated molecule and the repulsive 1–3 atom–atom interactions between C(1), (C1′) and O(1) will determine mainly the molecular scissor-mode frequency associated to the bending of the φ-angle. It is well known that in molecular systems with aromatic rings there may be a π-electron delocalization which can produce an extra conjugation energy contribution to the intramolecular region whose effect is a tendency to make the rings coplanar, which is not accounted for in the atom–atom terms. In our case, nevertheless, it is very likely that the phenone group weakens the conjugation between both phenyl rings and we have neglected this effect in principle, although in the last instance the correctness of this assumption will only be confirmed by the fact that satisfactory agreement between calculated and experimental crystal structures can be found with this intramolecular energy model.

This potential energy model has been applied to the lattice dynamics of DCBP, which has been obtained with the Born–von Karman formalism in the harmonic approximation with nine molecular degrees of freedom. The method of Taddei, Bonadeo, Marzzochi & Califano (1973) has been used to account for the internal degrees of freedom in which the dynamical problem is set up in terms of generalized normal coordinates of the isolated molecule, *i.e.* the mass-weighted rotations and translations around the inertia principal axes and the normal coordinates corresponding to molecular deformations, strictly speaking. In this way, the intermolecular dynamical matrix can be written as

$$D^{\text{inter}}_{\alpha\beta}(\mathbf{q}|kk') = \sum_{l'} \phi_{\alpha\beta}(0k, l'k') \exp[i\mathbf{q}(\mathbf{r}(l'k') - \mathbf{r}(0k))],$$

where the force constants are defined as the second derivatives of the *intermolecular* energy with respect to the molecular normal coordinates Q_α, $\alpha = 1, 9$, and (lk) labels the k molecule at the l unit cell

$$\phi_{\alpha\beta}(lk, l'k') = \partial^2 V^{\text{inter}}/[\partial Q_\alpha(lk)\partial Q_\beta(l'k')],$$

and the secular equation to obtain the lattice frequencies $\omega(\mathbf{q})$ and the polarization vectors $\mathbf{U}(\mathbf{q})$ can be written as

$$[\mathbf{D}^{\text{inter}}(\mathbf{q}) + \mathbf{D}^{\text{intra}}]\mathbf{U}(\mathbf{q}) = \omega^2(\mathbf{q})\mathbf{U}(\mathbf{q}),$$

where $\mathbf{D}^{\text{intra}}$ is a diagonal matrix whose elements are the second derivatives of the *intramolecular* energy with respect to each normal coordinate of the isolated molecule, *i.e.* the free-molecule squared frequencies (a frequency value of zero would correspond to the translational and rotational normal coordinates).

3.1. *Results*

Using the proposed crystal energy model, we have modelled the high- and low-temperature structures as the minimum-energy configurations corresponding to the chosen potential set. An energy-minimization process has been carried out starting at the experimental crystal structures of both phases and using the program *WMIN* (Busing, 1972). For the high-temperature phase, the maximum lattice parameter change during the process was 3.3% for the b parameter, a value for the monoclinic angle β of 99.3° was found and the molecule underwent a translation and rotation of 0.01 Å and 1.89°, respectively. The phenyl rings rotated 1.55° and the C(1)—C(7)—C(1′) φ angle varied 1.8° with respect to the experimental conformation. The results are very

similar for the low-temperature phase, where the maximum lattice parameter change is 2.7%, also for the b parameter, and a value of $\beta = 98.6°$ was obtained. Molecular translations and rotations are 0.005 Å and 1.49° and the phenyl rotations and the variation of the φ angle were 1.55 and 2.5°, respectively. These values are well within the usual tolerance obtained with semi-empirical potential parameters and constitute a first indication of the right choice of the potential model.

The lattice energies found for the equilibrium structures are -100.2 and $-98.9\,kJ\,mol^{-1}$ for the high- and low-temperature phase, respectively. This means that both phases are practically isoenergetic and probably the stability of each phase is driven by entropy effects. The small calculated energy difference between both phases is in the opposite sense to that expected from thermal stability arguments. This is probably due to the different molecular conformations (bond lengths and angles of the rigid parts of our model molecule) in both phases which would require the addition of a term for molecular deformation energy for a correct calculation of the crystal energy. In fact, we have calculated the energy of the low-temperature structure with our potential model, but modelling the molecule with the conformation which corresponds to the high-temperature phase and the resulting energy value in the minimization process is now $-100.3\,kJ\,mol^{-1}$, identical to the high-temperature value.

The orientation of the phenyl groups is expected to be due to the competition of inter- and intramolecular interactions. A calculation of the intramolecular energy as a function of the phenyl rotation angle is interesting as the minimum would correspond to the isolated molecular configuration. In Fig. 3 we have calculated this energy as a function of the dihedral angle between the phenyl best plane and the C(1)—C(7)—C(1′) plane with the C_2 molecular symmetry constraint, *i.e.* a value of zero would correspond to coplanarity of the phenyl groups. We can see that the most favourable conformation corresponds to both phenyl groups being perpendicular to the C(1)—C(7)—C(1′) plane and therefore the effect of the intermolecular field in the crystal is to rotate the rings in order to reduce the effective molecular volume in the crystal packing as much as possible.

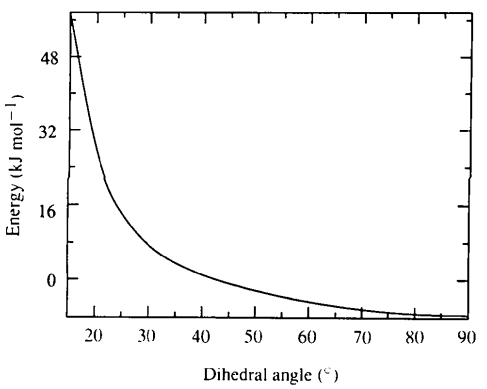

Fig. 3. Calculated intramolecular energy as a function of the dihedral angle between the phenyl rings and the C(1)—C(7)—C(1′) plane adopting the C_2 molecular symmetry.

The Raman spectra of the isolated molecule have been measured from a solution of DCBP in CCl_4 (Peretti & Ranson, 1979), where two lines at 55 and $90\,cm^{-1}$ have been obtained, although other lines expected for frequencies around and below $30\,cm^{-1}$ could not be observed because they were too near the exciting line. We have carried out a calculation of the frequencies at the molecular equilibrium conformation with our molecular model using the program *WMIN* and we have obtained frequency values of 55.3, 31.9 and $17.7\,cm^{-1}$. An analysis of the eigenvectors shows that the first mode corresponds to a scissor mode in which the C(1)—C(7)—C(1′) angle vibrates, whereas the second and the third are antisymmetric and symmetric phenyl twists (with respect to the molecular binary axis), respectively. Therefore, we can ascribe a scissor-mode character to the experimental line at $55\,cm^{-1}$. In fact, the same mode in the related compound 4,4′-dichlorodiphenyl sulfone has been measured at a very similar frequency of $62\,cm^{-1}$ (Ishii, Nakayama, Sakato & Kano, 1992). An interpretation remains to be given for the experimental higher frequency mode at $90\,cm^{-1}$. Our guess is that it corresponds to the excitation of another molecular degree of freedom not considered in our model, in particular the out-of-plane torsional movement of the phenyl rings with respect to the C(1)—C(7) bonds. A more exhaustive method to overcome this problem would be the adoption of a full internal molecular force field as a function of all internal coordinates using the internal modes below a certain frequency threshold in the way proposed by Filippini & Gramaccioli (1989), but this method requires the complete knowledge of such a force field and the setting up of this model is considerably more difficult.

We have calculated the crystal-lattice frequencies for both crystal phases for the energy-minimized configurations at the Brillouin zone centre with the WMIN program, which can be directly compared with the experimental Raman active modes (Peretti & Ranson, 1979). Tables 4(*a*) and (*b*) show the calculated and experimental frequencies for the high- and low-temperature phase, respectively, together with their symmetry representations. We can see that in both cases an acceptable fit between calculated and experimental data is achieved, given the simplicity of our molecular model, enough to allow us to interpret the Raman spectra in terms of the calculated eigenvectors. We can observe in both experimental spectra that the highest mode at 118.8 and $131\,cm^{-1}$ have no calculated counterpart. These modes probably correspond to the coupling of the free-molecule mode at $90\,cm^{-1}$ with the crystalline field which causes an increase in its frequency. Also, the highest A_g modes which are harder in our calculation

Table 4. *Calculated and experimental (Peretti & Ranson, 1979) lattice frequencies at $q = 0$ in cm^{-1} for DCBP*

Mode		calc.	exp.
(*a*) High-temperature phase			
1	B_g	–	118.8
2	A_g	132.8	106.9
3	A_u	118.9	–
4	B_g	101.1	100.8
5	B_u	99.8	–
6	A_u	73.2	–
7	B_g	71.7	79.6
8	A_g	68.4	52.8
9	B_g	64.0	66.8
10	A_u	63.7	–
11	B_u	50.7	–
12	A_g	48.4	42.0
13	B_g	46.1	42.0
14	B_g	36.7	34.4
15	A_g	29.3	26.8
16	B_u	25.8	–
(*b*) Low-temperature phase			
1	B_g	–	131.0
2	A_g	138.1	114.8
3	A_u	129.4	–
4	B_u	108.5	–
5	B_g	103.5	111.8
6	A_g	83.5	72.8
7	B_g	83.0	97.9
8	A_u	81.9	–
9	B_g	77.5	70.8
10	A_u	61.1	–
11	A_g	61.0	53.8
12	B_g	52.7	55.6
13	A_g	40.7	45.6
14	B_u	32.5	–
15	B_u	19.2	–
16	B_g	18.6	38.6

than the experimental values would probably soften if the coupling to the phenyl ring out-of-plane degree of freedom was allowed for. In Tables 5(*a*) and (*b*) we present the calculated mode eigenvectors for the high- and low-temperature phase, respectively, where molecular rotations and translations are referred to the centre-of-mass principal inertia axes (see Fig. 1). We can see in both spectra that there is a strong coupling between external and internal coordinates, so that neither mode can be ascribed a purely external or internal character. This coupling is particularly important for the phenyl twisting coordinates, in agreement with the fact that they were involved in the lowest frequency modes of the free-molecule calculation. We can also see that the modes with a larger contribution of phenyl rotations are those with higher frequencies, a result which seems surprizing given that this degree of freedom corresponds to the softest modes in the free molecule, and it can be explained as a hardening because of the crystalline field. This is an example of how the interpretations of experimental spectra made so often are only tentative and that a model calculation should be desirable in order to assign mode characteristics properly.

Lastly, a calculation of the dispersion curves at general wavevectors has been made with a computer code generated by us and using the method outlined in a previous section. Figs. 4(*a*) and (*b*) show the dispersion

Table 5. *Calculated eigenvector displacement components normalized to unity for the lattice modes at $q = 0$ of DCBP*

Molecular rotations and translations are expressed in radians and Å with respect to the principal inertia frame at the centre of mass (Fig. 1) and $\Delta\theta$ and $\Delta\varphi$ are the phenyl twist- and scissor-internal mode components, respectively.

Mode	R_x	R_y	R_z	T_x	T_y	T_z	$\Delta\theta$	$\Delta\varphi$
(*a*) High-temperature phase								
2	0.000	0.050	0.000	0.000	−0.330	0.000	−0.920	−0.205
3	0.000	−0.075	0.000	0.000	0.444	0.000	0.849	0.278
4	−0.218	0.000	−0.023	−0.014	0.000	−0.751	0.614	0.000
5	0.288	0.000	0.062	−0.014	0.000	−0.068	0.953	0.000
6	0.000	−0.170	0.000	0.000	0.690	0.000	−0.530	0.464
7	−0.302	0.000	−0.035	0.134	0.000	−0.304	−0.893	0.000
8	0.000	0.008	0.000	0.000	0.815	0.000	−0.306	0.492
9	0.648	0.000	0.034	0.088	0.000	−0.308	−0.690	0.000
10	0.000	−0.226	0.000	0.000	−0.765	0.000	0.324	−0.509
11	0.505	0.000	−0.802	−0.005	0.000	−0.023	0.317	0.000
12	0.000	0.140	0.000	0.000	−0.985	0.000	−0.061	0.085
13	0.461	0.000	−0.726	−0.424	0.000	0.197	−0.206	0.000
14	0.046	0.000	0.043	−0.968	0.000	0.027	−0.243	0.000
15	0.000	0.579	0.000	0.000	0.811	0.000	0.055	−0.060
16	0.605	0.000	0.030	0.012	0.000	0.057	−0.793	0.000
(*b*) Low-temperature phase								
2	0.000	0.033	0.000	0.000	−0.368	0.000	−0.894	−0.253
3	0.000	−0.055	0.000	0.000	0.446	0.000	0.844	0.294
4	−0.203	0.000	−0.054	0.002	0.000	0.026	−0.977	0.000
5	−0.264	0.000	−0.019	−0.005	0.000	−0.826	0.498	0.000
6	0.000	−0.028	0.000	0.000	0.546	0.000	−0.508	0.665
7	−0.520	0.000	−0.097	−0.439	0.000	0.297	0.663	0.000
8	0.000	−0.923	0.000	0.000	−0.278	0.000	−0.193	−0.184
9	−0.391	0.000	−0.055	0.294	0.000	−0.067	−0.868	0.000
10	0.000	0.055	0.000	0.000	−0.976	0.000	0.107	−0.182
11	0.000	−0.001	0.000	0.000	−0.752	0.000	0.447	−0.485
12	0.656	0.000	−0.422	−0.013	0.000	−0.174	−0.601	0.000
13	0.000	0.530	0.000	0.000	0.767	0.000	−0.241	0.271
14	0.656	0.000	−0.026	0.002	0.000	0.029	−0.754	0.000
15	0.207	0.000	0.597	−0.002	0.000	0.028	−0.775	0.000
16	0.206	0.000	0.044	−0.765	0.000	−0.184	−0.580	0.000

curves for the high- and low-temperature phase, respectively, in the main directions in reciprocal space. It is interesting to note that both phases are structurally stable, although a soft branch seems to appear in the high-temperature phase for $\mathbf{q} = 0.7\mathbf{b}^*$. This result has also been found for 4,4′-dichlorodiphenyl sulfone (Saito, Kikuchi & Ikemoto, 1992) which is isostructural, where in this case a soft mode has been found experimentally at $0.78\mathbf{b}^*$ (Etrillard, Sougoti, Toudic & Bourges, 1994). Therefore, it seems that this soft-mode instability is closely related to the structure of this family of compounds, although it takes effect only in some cases to cause a soft-mode driven transition. This is also the case for the A_2BX_4 family of compounds where calculations show a structural instability (Etxebarria, Pérez-Mato & Madariaga, 1992), although only some members show a soft-mode transition. In our case, the high-temperature phase transition is associated with a wavevector close to $0.5a^*$, although no indication of a soft branch can be observed at this point in our calculated dispersion branches for the high-temperature phase.

We have also calculated the lattice dynamics under pressure in order to study a possible pressure-induced

phase transition. The calculation of the dispersion curves has been carried out by introducing a pV energy term in the energy minimization procedure in order to obtain the equilibrium configuration corresponding to a given temperature, and the lattice dynamics calculations have been carried out in the pressure range 0–20 kbar (0–2×10^8 Pa); the effect of pressure is to harden the lattice frequencies of the crystal, but no structural instability seems to appear.

We have also tried to obtain evidence of the phenyl rotation through an analysis of the experimental atomic thermal parameters. For this purpose we used the program *THMA* (Dunitz, Schomaker & Trueblood, 1988) which permits a generalized **TLS** fit, allowing for one additional mean-square parameter per non-rigid group to account for the twist motion. In our case we have tried to fit an overall molecular **TLS** set of rigid-body tensors plus an additional mean-square amplitude for the phenyl twist around the axis defined by the C(7)—C(1) bond. The values obtained for the diagonal components of the translational and rotational thermal tensors in the principal inertia axes (Fig. 1) are $T_{11} = 162\ (5)$, $T_{22} = 121\ (6)$, $T_{33} = 135\ (9) \times 10^{-4}$ Å^2 and $L_{11} = 56\ (3)$, $L_{22} = 3\ (1)$, $L_{33} = 10\ (1) \times 10^{-4}$ rad^2,

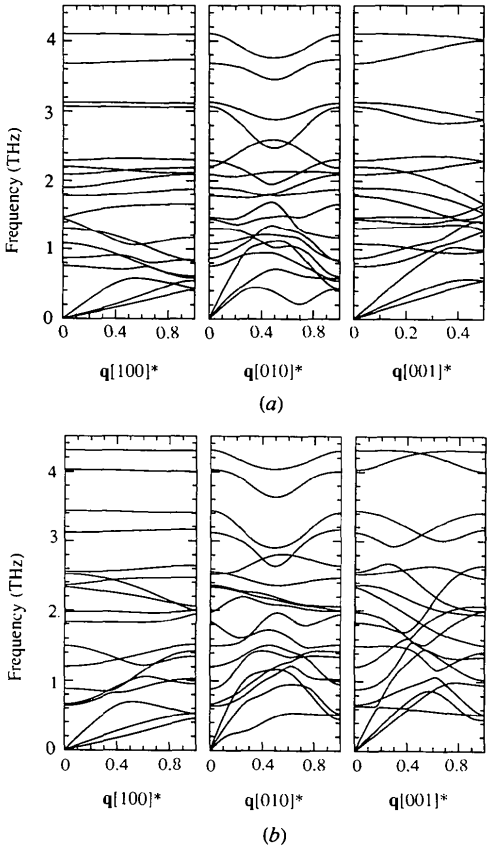

Fig. 4. Calculated (*a*) high- and (*b*) low-temperature dispersion curves in THz (1 THz = 33.35 cm^{-1}) for the three basic reciprocal directions with **q** expressed in 2π units of the basic reciprocal vectors.

respectively, whereas the mean-square internal amplitude gave an unrealistic negative value of $\langle\theta^2\rangle = -11\ (8) \times 10^{-4}$ rad^2 with an overall R-fit disagreement factor of 0.10. This result may be ascribed to the rather low number of independent atomic U_{ij}'s in the **TLS** fit process, coupled to the fact that the contributions of $\langle\theta^2\rangle$ may be largely absorbed into the L_{11} component of the librational tensor. An extreme example which can illustrate this effect is biphenyl, located at an inversion centre, where the internal twist parameter would be accounted for completely by the librational tensor component along the molecular axis because the information regarding the phase of the relative motion of each phenyl ring is not present in the diffraction data. We tried to repeat the **TLS** fit, omitting the O atom, and the resulting values for the internal amplitude and the L_{11} librational component were very different from the previous ones, indicating that the rigid-body parameters are not well determined by the available experimental data, in agreement with the above explanation.

In order to obtain an independent estimation of the thermal **TLS** tensors we have also carried out a lattice-dynamical calculation of these tensors by means of a dense sampling inside the Brillouin zone (Filippini, Gramaccioli, Simonetta & Suffritti, 1976), also obtaining the thermal amplitudes corresponding to the internal degrees of freedom, namely $\langle\theta^2\rangle$ and $\langle\varphi^2\rangle$. The values obtained for the diagonal components are $T_{11} = 155$, $T_{22} = 140$, $T_{33} = 122 \times 10^{-4}$ Å^2 and $L_{11} = 31$, $L_{22} = 5$, $L_{33} = 11 \times 10^{-4}$ rad^2, and the calculated internal components are $\langle\theta^2\rangle = 45$ and $\langle\varphi^2\rangle = 7 \times 10^{-4}$ rad^2 for the twist and scissor displacements, respectively. We can see now that we obtain a realistic value for the twist mean-square amplitude, which turns out to be slightly larger than the L_{11} librational component, whereas for the rest of the tensor components the agreement with those obtained from the **TLS** fit of the experimental data is very good.

We must notice that a good lattice-dynamical model can give more reliable values for the internal mean-square amplitudes than a **TLS** fit, allowing for internal motion. The $\langle\theta^2\rangle$ value obtained from the lattice dynamics can be unambiguously ascribed to the internal twist of the non-rigid group with respect to the body of the molecule, whereas a similar interpretation of the corresponding quantity obtained in a **TLS** fit always suffers from an indetermination whose magnitude is the librational tensor component along the direction of the twist rotation axis (Dunitz, Schomaker & Trueblood, 1988).

4. Concluding remarks

The existence of two phase transitions for DCBP at low temperatures has been confirmed by X-ray diffraction techniques and the crystal structure of the low temperature phase at 140 K has been determined. The three

different phases have similar basic unit cells and the difference between the room-temperature and the low-temperature (140 K) structures resides in the different packing of the molecular stacks according to a *C*- or *I*-centring, and, in both cases, the relative position of the molecules along *b*- and *c*-directions as well as the molecular conformation are similar. Also, in both cases, the set of intermolecular contacts is alike, except for a shorter Cl···Cl distance at 140 K, explaining the isoenergetic character of both structures.

Unlike biphenyl and 4-4′-dichlorophenyl sulfone, the phase transitions in DCBP do not seem to originate from conformational changes in the molecules as a consequence of competition between intra- and intermolecular interactions. Also, the transition mechanism seems to be different from the former cases, where a soft-mode is present at the phase transition. In our case, the calculated dispersion curves do not show any softening for wavevectors close to the modulation vector of the intermediate phase, indicating that both structures correspond to well-defined minima of the energy hypersurface as a function of the structural parameters, in agreement with Landau theory predictions for first-order transitions.

Looking at the room-temperature structure we can see that if we shift the molecular rows parallel to the *c*-direction at $x = \frac{1}{2}$, an amount of $\frac{1}{2}c$, we obtain the low-temperature structure, changing from *C*- to *I*-packing. Taking into account the superlattice reflections that appear in the intermediate phase, which correspond to a periodicity of almost $2a(\mathbf{q} = 0.52\mathbf{a}^*)$, we must consider molecular displacements with the same periodicity in order to develop a model for the phase transition. A possible model might consist in alternate displacements of molecular rows parallel to the *c*-direction at $x = 0$ and $x = 1$ with an (almost) opposite phase (see Fig. 2*a*), so that a displacement of $\frac{1}{2}c$ would also result in the low-temperature phase. For intermediate displacements between 0 and $\frac{1}{2}c$ we would have a modulated primitive lattice where neither the *C*- nor the *I*-centring are fulfilled, in agreement with the experimental evidence for the intermediate phase. The continuous evolution of the intensities of the *C*- and *I*-extinction reflections, which seems to suggest an also continuous transition from the high- to the low-temperature structure in the range of the intermediate phase, could therefore be explained within this model as a gradual displacement of molecular rows between both extreme configurations. Nevertheless, this model does not seem to explain the observed extinction rule for the superstructure reflections at (*hkl*) layers, *l* even. Assuming a modulation-molecular displacement along the *c*-direction and $\mathbf{q} \simeq 0.5\mathbf{a}^*$, one can arrive at the following general extinction rule: $\mathbf{H}(\delta\mathbf{c} + \mathbf{a}) = (2n + 1)/2$, where δ is the relative molecular displacement between alternate molecular rows at $x = 0$ and $x = 1$ ($\delta = 1$ would correspond to the low-temperature structure). For the satellite reflections $\mathbf{H} \simeq (h + \frac{1}{2}, k, l)$ this extinction condition leads to $h + \frac{1}{2} + \delta l = (2n + 1)/2$, *i.e.* δl must be an integer. Therefore, satellite extinction for even *l* requires that $\delta = \frac{1}{2}$, therefore, alternate molecular rows must be displaced $\frac{1}{4}c$, half-way between the high- and low-temperature structures, in contradiction with a continuous displacement hypothesis. Assuming a modulation periodicity of $2a$, the model structure shown in Fig. 5 is for the intermediate phase where the molecules have been shifted $\frac{1}{4}c$, giving rise to a duplicated primitive unit cell with space group $P2/c$ ($Z = 8$), where the inversion centre is located at $(\frac{1}{4}, 0, \frac{1}{4})$.

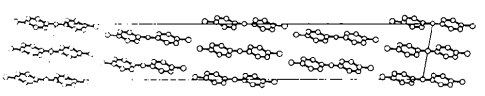

Fig. 5. Projection along the *b*-direction of the structure of the proposed intermediate phase with $\pm\frac{1}{4}c$ displacements of the DCBP molecules.

A more complicated model, in which, within the range of the intermediate phase, the molecules in the crystal would gradually perform the transition from *C*- to *I*-packing *via* discrete displacements of $\pm\frac{1}{4}c$ in a sort of coexistence of the high- and the low-temperature structure, could perhaps explain all the experimental features, even the abnormally large satellite reflection profiles. More detailed experimental work will be carried out in future in order to characterize properly the intermediate phase.

Another plausible explanation which could also account for all the experimental diffraction characteristics of the intermediate phase would be the coexistence in this phase of domains of *C*- and *I*-centring with zones of alternate centred cells in the form *CICICI*, which would give rise to the presence of satellite reflections. When decreasing the temperature the domains of *C*-centring would gradually decrease in size and the *I*-domains would increase going through states of alternate centring in order to make the transition to the low-temperature phase. Within this hypothesis, the small departure of the experimental modulation wavevector from the commensurate value might find an explanation as discommensuration effects at the domain boundaries.

AC thanks the Spanish DGICYT for financial support through the projects PB92-114-C04-04 and PB91-0446.

References

BATES, J. B. & BUSING, W. R. (1974). *J. Chem. Phys.* **60**, 2414–2419.
BUSING, W. R. (1972). *Acta Cryst.* A**28**, S252.
CAILLEAU, H. (1986). *Incommensurate Phases in Dielectrics*, edited by R. BLINC & A. P. LEVANYUK, Vol. 2, ch. 12, Modern Problems in Condensed Matter Sciences. Amsterdam: North-Holland.
COSIER, J. & GLAZER, A. M. (1986). *J. Appl. Cryst.* **19**, 105–107.
COX, S. R., WILLIAMS, D. E. & HSU, L. (1981). *Acta Cryst.* A**37**, 293–301.
CRIADO, A. & LUTY, T. (1993). *Phys. Rev. B*, **48**, 12419–12424.
CRIADO, A. & MARQUEZ, R. (1988). *Acta Cryst.* A**44**, 76–78.

CRIADO, A. & MUÑOZ, A. (1993). *Acta Cryst.* B**49**, 726–729
DUNITZ, J. D., SCHOMAKER, V. & TRUEBLOOD, K. N. (1988). *J. Phys. Chem.* **92**, 856–867.
ECOLIVET, C., BERTAULT, M., MIERZEJEWSKI, A. & COLLET, A. (1987). *Dynamics of Molecular Crystals*, edited by J. LACOMTE. Amsterdam: Elsevier Science Publishers.
ETRILLARD, J., SOUGOTI, M., TOUDIC, B. & BOURGES, P. (1994). Private communication.
ETXEBARRIA, I., PÉREZ-MATO, J. M. & MADARIAGA, G. (1992). *Phys. Rev. B*, **46**, 2264–2274.
FILIPPINI, G. & GAVEZZOTTI, A. (1993). *Acta Cryst.* B**49**, 868–880.
FILIPPINI, G. & GRAMACCIOLI, C. M. (1989). *Acta Cryst.* A**45**, 261–263.
FILIPPINI, G., GRAMACCIOLI, C. M., SIMONETTA, M. & SUFFRITTI, G. B (1976). *Acta Cryst.* A**32**, 259–264.
GRANGER, M. M. & COILLOT, M. F. (1985). *Acta Cryst.* C**41**, 542–543.
ISHII, K., NAKAYAMA, H., SAKATO, T. & KANO, H. (1992). *J. Phys. Soc. Jpn*, **61**, 2317–2326.
KIRIN, D. & PAWLEY, G. S. (1982). *Chem. Phys Lett.* **85**(3), 298–301.
MUÑOZ, A. & CRIADO, A. (1992). *Acta Cryst.* B**48**, 302–306.
PERETTI, P. & RANSON, T. (1979). *J. Raman Spectrosc.* **8**, 209–212.
PERTSIN, A. J. & KITAIGORODSKY, A. I. (1987). *The Atom–Atom Potential Method*, Springer Series in Chemical Physics. Berlin: Springer-Verlag.
PLAKIDA, N. M., BIELUSHKIN, A. V., NATKANIEC, I. & WASIUTYNSKI, T. (1983). *Phys. Status Solidus B*, **118**, 129–133.
PUSIOL, D. J., WOLFENSON, A. E. & BRUNETTI, A. H. (1989). *Phys Rev. B*, **40**, 2523–2528.
SAITO, K., KIKUCHI, K. & IKEMOTO, I. (1992). *Solid State Commun.* **81**, 241–243.
SHIELDS, K. G. & KENNARD, C. H. L. (1977). *J. Chem. Soc. Perkin Trans* 2, p. 463.
STEWART, J. M., KRUGER, G. J., AMMON, H. L., DICKINSON, C. W. & HALL, S. R. (1972). *The XRAY72 System*, Version of June 1972. Technical Report TR-192. Computer Science Center, Univ. of Maryland, College Park, USA.
TADDEI, G., BONADEO, H., MARZZOCHI, M. P. & CALIFANO, S. (1973). *J. Chem. Phys.* **56**, 966–978.
WILLIAMS, D. E. (1967). *J. Chem. Phys.* **47**, 4680–4684.
WILLIAMS, D. E. & STARR, T. L. (1977). *Comput. Chem.* **1**, 173–177.
WOLFENSON, A. E., PUSIOL, D. J. & BRUNETTI, A. A. (1990). *Z. Naturforsch. Teil A*, **45**, 334–339.
ZÚÑIGA, F. J., PÉREZ-MATO, J. M. & BRECZEWSKI, T. (1993). *Acta Cryst.* B**49**, 1060–1068.

Acta Cryst. (1995). B**51**, 888–892

Crystal Structures and Photochemistry of Triphenylphosphine Oxide Complexes of Ethyl Hydrogen 9,10-Dihydro-9,10-ethenoanthracene-11,12-dicarboxylate

BY RAY JONES, ZHAOQING LIU, JOHN R. SCHEFFER AND JAMES TROTTER

Department of Chemistry, University of British Columbia, Vancouver, BC, Canada V6T 1Z1

(*Received* 8 *July* 1994; *accepted* 17 *January* 1995)

Abstract

The detailed course of the photochemical rearrangement reactions of dibenzobarrelenedicarboxylates has been studied by crystal structure analyses of two complexes of triphenylphosphine oxide (1) with the monoester ethyl hydrogen 9,10-dihydro-9,10-ethenoanthracene-11,12-dicarboxylate (2), and by correlation of the crystal structure data with photochemical behaviour. Crystal data: $T = 294$ K, Cu $K\alpha$, $\lambda = 1.54178$ Å. (1.2), $C_{18}H_{15}OP.C_{20}H_{16}O_4$, $M_r = 598.63$, $P\bar{1}$, $a = 13.501(1)$, $b = 14.845(1)$, $c = 8.5190(6)$ Å, $\alpha = 102.21(1)$, $\beta = 98.68(1)$, $\gamma = 68.70(1)°$, $Z = 2$, $R = 0.039$ for 4546 reflections with $I > 3\sigma(I)$; (1.2).0.5toluene, $C_{18}H_{15}OP.C_{20}H_{16}O_4.0.5C_7H_8$, $M_r = 644.71$, $P2_1/n$, $a = 8.546(2)$, $b = 28.164(5)$, $c = 14.368(2)$ Å, $\beta = 98.81(2)°$, $Z = 4$, $R = 0.052$ for 3462 reflections. Both crystals contain pairs of molecules linked by O—H···O hydrogen bonds, with dimensions and conformations similar to those of previously studied analogues. In the unsolvated crystal the ester group of the monoester is fully conjugated with the C(11)=C(12) double bond [C=C—C=O torsion angle = $-179.6(2)°$, $\cos^2$(angle) = 1.0], but the acidic group is non-conjugated [109.0(3)°, 0.11]. In the toluene solvate the opposite is the case, the ester group being non-conjugated [110.5(5)°, 0.12], and the acid group conjugated [$-13.8(6)°$, 0.94]. The different amounts of photoproducts formed in the solid-state photolyses can be correlated with these conformational differences.

Introduction

Triphenylphosphine oxide (1) is a good hydrogen-bond acceptor and forms crystalline complexes with a variety of hydrogen-bond donors (Etter & Baures, 1988). The present paper studies the influence that co-crystallization might have on the photochemical reactivity of the 9,10-ethenoanthracene compound (2). (2) and its derivatives undergo di-π-methane photorearrangements in a variety of solid and liquid media, to give (3) and (4) [isolated as diesters after diazomethane workup (Gudmundsdottir, Scheffer & Trotter, 1994; Gudmundsdottir, Li, Scheffer, Rettig & Trotter, 1994)]; the ratio in which these photoproducts are formed (and the optical purity of any chiral products) can be correlated with the molecular structure of the reactant, and in particular with the amount of conjugative interaction of the ester and acid